PAPER

Check for updates

Modified carbon felt made using Ce$_x$A$_{1−x}$O$_2$ composites as a cathode in electro-Fenton system to degrade ciprofloxacin†

Yi Li, [ID] *[a] Jingjing Han,[a] Xueyue Mi,[b] Xinqiang Mi,[c] Yanan Li,[a] Suge Zhang[a] and Sihui Zhan[b]

Carbon felt (CF) was modified by Ce$_x$A$_{1−x}$O$_2$ (A = Zr, Cu and Ni) and the role of these Ce$_x$A$_{1−x}$O$_2$/CF (A = Zr, Cu and Ni) cathode materials in the oxidative degradation of antibiotic ciprofloxacin (CIP) was investigated in the electro-Fenton system. SEM, BET, TEM, XPS, TOC, HPLC-MS, CV and EIS were used to understand the characteristics of these cathode materials. The CIP degradation efficiency of the Ce$_x$A$_{1−x}$O$_2$/CF (A = Zr, Cu and Ni) cathode was better than that of pure CF, and 2.0 wt% Ce$_{0.75}$Zr$_{0.25}$O$_2$/CF was the most effective cathode material for degradation of CIP. It reached 100% degradation efficiency of CIP after 1 h and almost total mineralization (97.45%) after 6 h, owing to synergistic effects from the predominant role of homogeneous ·OH produced electrocatalytically through the Fenton reaction of Fe^{2+} and H$_2$O$_2$ and heterogeneous ·OH produced *via* the Fenton-like reaction of Ce^{3+} and H$_2$O$_2$ and the electrocatalytic activity of Ce$_{0.75}$Zr$_{0.25}$O$_2$ composite and the strong electrosorption of carbon felt. A possible path of CIP degradation was proposed in the paper.

1 Introduction

In the last few years, environmental pollution has been paid much attention in the world, and the treatment of antibiotic wastewater is one of the major problems.[1–3] Ciprofloxacin (CIP) is a fluoroquinolone antibiotic and its concentration has been detected up to 31 mg L^{-1} in waste effluents from pharmaceutical manufacturers.[4,5] And ciprofloxacin is more difficult for microorganisms to degrade and cannot be effectively removed by conventional water treatment process.[6] Therefore, it is important to find an effective method for removing ciprofloxacin from the environment.

Advanced oxidation processes (AOPs)[7–11] are based on *in situ* production of hydroxyl radicals (·OH). As the second strongest oxidant after fluorine,[12,13] ·OH is able to non-selectively react with persistent organic pollutants (POPs) and degrade them into CO$_2$, H$_2$O and inorganic ions. Among AOPs, electrochemical advanced oxidation processes (EAOPs) have received much attention because of their efficiency in the destruction of toxic and/or bio-refractory organic pollutants, environmental

friendliness and computability and widespread applications.[14–17] Recently, the most common EAOP based on Fenton chemistry is the electro-Fenton (EF) process.[18,19] An efficient cathode material is crucial to the EF system. At present, it has been reported that the cathode materials with excellent performance are gas diffusion electrode,[20–22] graphite electrode[23] and three-dimensional porous electrode.[24] The biggest advantage of the three-dimensional porous electrode is the larger specific surface area, which greatly increases the electrode reaction area, and thus increases the reaction rate. Carbon felt (CF), a kind of three-dimensional porous electrode, is often used as electrode material in the EF process[25] and all-vanadium redox flow battery[26] because of their low cost, high stability, high conductivity, corrosion resistance, and high surface area. So we choose carbon felt as the supporting material to load Ce$_x$A$_{1−x}$O$_2$ composites (A = transition metals) by using as cathode to degrade ciprofloxacin by the electro-Fenton process.

Over the past decades, cerium dioxide (CeO$_2$) has received extensive attention, which possesses considerable oxygen storage capacity owing to the redox cycling between Ce^{3+} and Ce^{4+}. However, pure CeO$_2$ shows poor stability and is prone to sintering at high temperature which leads to reducing the catalytic activity.[27] In order to further improve the performance of oxygen storage, oxygen release and thermal stability, we modified pure CeO$_2$. When the transition metal ions are doped into CeO$_2$ producing Ce$_x$A$_{1−x}$O$_2$ (A = transition metals) composites, the cerium ion will be replaced by the transition metal ions which results in producing some lattice defects. This

[a]*Tianjin Key Laboratory of Molecular Optoelectronic Sciences, Department of Chemistry, School of Science, Tianjin University & Collaborative Innovation Center of Chemical Science and Engineering (Tianjin), Tianjin 300072, China. E-mail: liyi@tju.edu.cn*

[b]*College of Environmental Science and Engineering, Nankai University, Tianjin 300071, China*

[c]*Befar Group Corporation, Binzhou 256601, China*

makes the migration channel of oxygen ions in the crystal lattice become relatively large, which can effectively reduce the diffusion resistance of oxygen in the crystal lattice and improve the ability of oxygen activity. And the conversion between different valence states of the transition metal ions is helpful to form oxygen vacancies. Thus the electro-catalytic activity of CeO_2 is improved. $Ce_xA_{1-x}O_2$ composites can be used for the treatment of automobile tail gas,[28] the transformation of vanadium lithium battery[29] and the degradation of antibiotics of carbon or graphite felt loaded iron oxide as cathode by EF system.[30–32] However, it is not common that $Ce_xA_{1-x}O_2$/CF composites are used as cathode to degrade antibiotics in the EF process.

In this paper, $Ce_xA_{1-x}O_2$/CF (A = Zr, Cu and Ni) composites were obtained by impregnating the CF into $Ce_xA_{1-x}O_2$ solid solution and then dried and calcined. And the carbon felt modified by $Ce_xA_{1-x}O_2$ (A = Zr, Cu and Ni) composites was used as cathode to degrade CIP in EF system, respectively. Compared to the pure CeO_2, $Ce_xA_{1-x}O_2$/CF (A = Zr, Cu and Ni) composites have many superior aspects: (1) $Ce_{0.75}Zr_{0.25}O_2$, $Ce_{0.90}Cu_{0.10}O_2$ and $Ce_{0.85}Ni_{0.15}O_2$ catalysts have more oxygen vacancies and higher oxygen storage capacity (OSC). (2) The electrocatalytic activities of $Ce_{0.75}Zr_{0.25}O_2$, $Ce_{0.90}Cu_{0.10}O_2$ and $Ce_{0.85}Ni_{0.15}O_2$ composites are stronger than that of pure CeO_2. (3) CF has strong electrosorption behavior. Above synergies gained the efficient degradation of CIP. And intermediates of CIP degradation were identified by using HPLC-MS analysis to propose a reasonable mineralization pathway.

2 Experimental

2.1 Chemicals

All chemicals are analytical grade and used without further purification. Ciprofloxacin, $C_{17}H_{18}FN_3O_3$ (≥98% purity), was purchased from Alfa Aesar, UK. Na_2SO_4, $FeSO_4·7H_2O$, $Ce(NO_3)_3·6H_2O$, $Zr(NO_3)_4·5H_2O$, $Cu(NO_3)_2·3H_2O$ and $Ni(NO_3)_2·6H_2O$ were purchased from Shanghai Aladdin Industrial Co. Methanol and phosphoric acid used in preparation of HPLC eluents were obtained from Sigma-Aldrich.

2.2 Preparation of the $Ce_xA_{1-x}O_2$/CF (A = Zr, Cu and Ni) composite electrodes

The $Ce_xA_{1-x}O_2$/CF composites were prepared by impregnating the CF into $Ce_xA_{1-x}O_2$ solid solution and then dried and calcined.[33] Before the experiment, the CF should be treated with acid to enhance its wettability and eliminate impurities.[34] The tri-dimensional carbon-felt (6 cm × 3 cm each side, 0.5 cm in width-Carbone Lorraine) was soaked in 10% H_2O_2 at 90 °C for 3 h and then marinated in 10% HCl at 90 °C for 1 h. At last, it was rinsed with distilled water and dried at 60 °C for overnight. CF was immersed into $Ce(NO_3)_3·6H_2O$ and $Zr(NO_3)_4·5H_2O$ solutions (quality ratio of 3 : 1) accompanied by addition of $NH_3·H_2O$ diluted solutions until the pH was 10 and the solutions went through ultrasound for half an hour. Subsequently, the sample was dried at 70 °C for 12 h and then heated to 500 °C for 5 h under a flow of N_2. When the quantity of CF was 1 g,

24 mg $Ce(NO_3)_3·6H_2O$ and 8 mg $Zr(NO_3)_4·5H_2O$ was dissolved in 20 mL deionized water to prepare a 2.0 wt% precursor solution. In order to get the best load capacity, 1.0, 1.5, 2.5, and 3.0 wt% of $Ce_{0.75}Zr_{0.25}O_2$ composites loaded on CF were investigated, respectively. According to the above description, the $Ce_{0.75}Zr_{0.25}O_2$/CF composite electrodes were synthesized. Preparation of the $Ce_{0.90}Cu_{0.10}O_2$/CF composite electrodes and the $Ce_{0.85}Ni_{0.15}O_2$/CF composite electrodes employed the same method. However, the load capacity on CF was 1.0, 1.5, 2.0, 2.5, and 3.0 wt% of $Ce_{0.90}Cu_{0.10}O_2$ composite, respectively. The load capacity of $Ce_{0.85}Ni_{0.15}O_2$ composite on CF was 0.14, 0.30, 0.45 and 0.60 wt%, respectively. CF without modification by $Ce_xA_{1-x}O_2$ was also heated to 500 °C for 5 h for comparison.

2.3 Electrolytic system

The EF degradation of CIP was conducted in a cylindrical glass cell of 250 mL capacity at room temperature (23 ± 2 °C) and pH = 3.0. The aqueous solution was 50 mg L^{-1} CIP solution and contained 0.1 mmol L^{-1} Fe^{2+} and 0.05 mol L^{-1} Na_2SO_4 solution. The solution was continuously saturated by bubbling compressed O_2 at the rate of 100 mL min^{-1}. The distance between the Pt plate (1 cm × 0.5 cm) as anode and $Ce_xA_{1-x}O_2$/CF composites as cathode was 1.0 cm. There was a magnetic mixer to ensure the uniformity of the electrolysis during the EF process.

2.4 Analytical procedures

Electrochemical activities of $Ce_xA_{1-x}O_2$/CF composite electrodes were evaluated by using cyclic voltammetry (CV) and electrochemical impedance spectroscopy (EIS) in a traditional three-electrode cell. $Ce_xA_{1-x}O_2$/CF composites were the working electrodes. Pt plate and saturated calomel electrode (SCE) were used as the counter electrode and the reference electrode, respectively.

The concentration of CIP at a certain time was detected by reversed-phase high performance liquid chromatography (HPLC) using a Merck Lachrom liquid chromatograph equipped with a L-7100 pump, fitted with a Purospher RP-18, 5 μm, 25 cm × 4.6 mm (i.d.) column at 40 °C, and coupled with a L-7455 photodiode array detector selected at optimum wavelengths of 250 nm. The mobile phase was a methanol/ 0.06 mmol L^{-1} H_3PO_4 55 : 65 (v/v). A flow rate was 0.8 mL min^{-1}. Samples of 20 μL were injected into the HPLC and the measurements were controlled through EZ-Chrom Elite 3.1 software.

The formed intermediates of CIP degradation to get a reasonable mechanism were identified by the high performance liquid chromatography-mass spectrometry (HPLC-MS, Waters XEVO TQS analyzer) connected with ESI source. The Waters Acquity UPLC BEH C18 column (2.1 mm × 1.8 mm, 1.7 μm) was employed. The temperature of the column was 40 °C. A gradient elution was applied using the mobile phase formed by 0.5% methane acid aqueous solution and acetonitrile (80% : 20%) at the flow rate of 0.5 mL min^{-1}, 10 min run. The injection volume was 20 μL and UV detector was set up at 276 nm. ESI source conditions were as follows: capillary voltage,

sample cone voltage and extraction cone voltage were 2000, 45 and 4 V, respectively; the source block and desolvation temperatures were 100 and 250 °C, respectively and the desolvation and nebulizer gas (N_2) flow rate was 600 L h^{-1}. Total compounds mass spectra were obtained in the positive ion mode between m/z 100 and 400.

Scanning electron microscopy (SEM) images and mapping analysis were carried out on SU8010 field emission to obtain the microstructures and the composition of $Ce_xA_{1-x}O_2$/CF composite electrodes. Transmission Electron Microscope (TEM) characterized the morphology and structure of the product. The nitrogen adsorption–desorption isotherm was measured at 77 K using the surface area and pore-size analyzer (Quantachrome Autosorb iQ-MP). The total surface area was calculated from the Brunauer–Emmett–Teller (BET) method and the pore size distribution data was calculated using the density functional theory (DFT) method based on the adsorption and desorption data. X-ray Photoelectron Spectroscopy (XPS) was used ESCA X PHI-1600 ray photoelectron spectroscopy of the United States PE company to obtain the data of the binding energies of Ce 3d, Zr 3d, Cu 2p, Ni 2p, C 1s and O 1s, and 284.6 eV was the referencing of C 1s peak. The removal of the total organic carbon (TOC, TOC-VCPH, Japan) can assess the mineralization degree of treated solutions.

3 Results and discussion

3.1 Characterizations of the $Ce_xA_{1-x}O_2$/CF composite electrodes

3.1.1 SEM and mapping analysis. The surface morphologies of CF and $Ce_xA_{1-x}O_2$/CF (A = Zr, Cu and Ni) composites are characterized by SEM. As shown in Fig. 1a, we can see that the surface of the carbon fibers becomes excessively rough and has many grooves after the acid treatment. It can improve the specific surface area of the electrode and thus increase the active surface area, and further promote the oxygen reduction reaction. As shown in Fig. 1b–d, $Ce_xA_{1-x}O_2$ (A = Zr, Cu and Ni) nanoparticles are randomly loaded on the surface of the CF fibers. Fig. 1e–p presents the mapping analysis of 2.0 wt% $Ce_{0.75}Zr_{0.25}O_2$/CF composite, 2.5 wt% $Ce_{0.90}Cu_{0.10}O_2$/CF composite and 0.45 wt% $Ce_{0.85}Ni_{0.15}O_2$/CF composite, respectively. From Fig. 1e–h, C, Ce, Zr and O evenly disperses on the scanning area, which indicates excellent distribution of CeO_2 and ZrO_2 on CF. For $Ce_{0.90}Cu_{0.10}O_2$/CF composite, we can see C, Ce, Cu and O also disperses on the scanning area from Fig. 1i–l. The corresponding elemental mapping of $Ce_{0.85}Ni_{0.15}O_2$/CF composite shows uniform spatial element distribution of C, Ce, Ni and O from Fig. 1m–p. By SEM and the mapping analysis, carbon fiber in carbon felt was successfully modified by $Ce_{0.75}Zr_{0.25}O_2$, $Ce_{0.90}Cu_{0.10}O_2$ and $Ce_{0.85}Ni_{0.15}O_2$, respectively.

3.1.2 TEM analysis. As shown in Fig. 2, the morphologies and structure of the 2.0 wt% $Ce_{0.75}Zr_{0.25}O_2$/CF composite, 2.5 wt% $Ce_{0.90}Cu_{0.10}O_2$/CF composite and 0.45 wt% $Ce_{0.85}Ni_{0.15}O_2$/CF composite are investigated by HR-TEM. HR-TEM images indicate that $Ce_{0.75}Zr_{0.25}O_2$, $Ce_{0.90}Cu_{0.10}O_2$ and $Ce_{0.85}Ni_{0.15}O_2$ nanoparticles have good crystallinity. From Fig. 2a, the lattice fringes of 0.307 nm were assigned to the (1 1 1) plane of
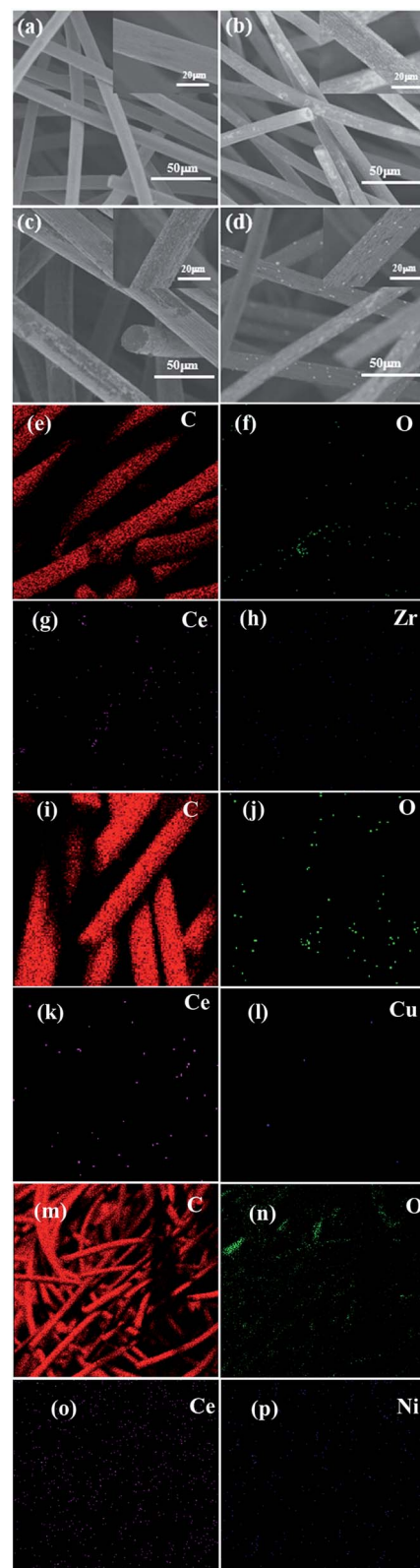

Fig. 1 SEM images at different magnifications and mapping analysis of CF (a), 2.0 wt% $Ce_{0.75}Zr_{0.25}O_2$/CF (b, e, f, g, h), 2.5 wt% $Ce_{0.90}Cu_{0.10}O_2$/CF (c, i, j, k, l), 0.45 wt% $Ce_{0.85}Ni_{0.15}O_2$/CF (d, m, n, o, p).
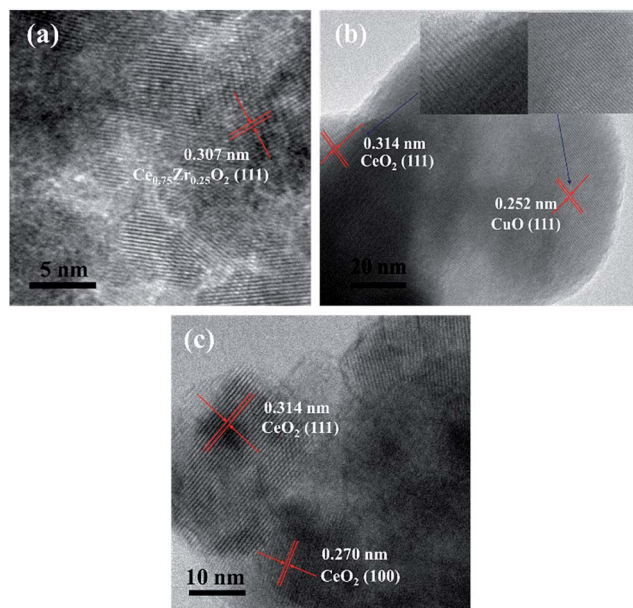
Fig. 2 HR-TEM images of 2.0 wt% $Ce_{0.75}Zr_{0.25}O_2$/CF composite (a), 2.5 wt% $Ce_{0.90}Cu_{0.10}O_2$/CF composite (b) and 0.45 wt% $Ce_{0.85}Ni_{0.15}O_2$/CF composite (c).

$Ce_{0.75}Zr_{0.25}O_2$.[35,36] It was shown in Fig. 2b, the most frequently observed reflection with a *d* spacing value of 0.314 nm corresponds to crystal lattice plane (1 1 1) of CeO_2. The reflection with a spacing value of 0.252 nm, attributable to the lattice plane (1 1 1) of CuO, can also be identified. Fig. 2c showed lattice fringes of CeO_2 (*d* = 0.314 nm and 0.270 nm) correspond to (1 1 1) and (1 0 0) lattice plane of CeO_2. However, HR-TEM image did not reveal any evidence of NiO particles which indicated that the NiO crystallites were highly dispersed and the particle size was too small not to be observed.[37]

3.1.3 XPS analysis. To understand the elemental composition and functional groups on CF and the $Ce_xA_{1-x}O_2$/CF composite, the surface chemistry of the electrodes was investigated by X-ray photoelectron spectroscopy (XPS) measurement. Fig. 3 shows the XPS spectra of C 1s for different electrode composites. On the basis of the reported literature,[38] the main peak at 284.7 eV is assigned to the graphitized carbon and the rest of the peaks correspond to, the defective carbon (285.3 eV), –OH groups (286.0 eV) and C=O groups (287.0 eV). And we find that there is an irregular peak in 282.0 eV corresponding to C–O–C groups.[39] This may be due to the introduction of functional groups in the treatment of CF.

The XPS spectra of O 1s for electrode composites are given in Fig. 4. The O 1s XPS spectra are scientifically resolved into two XPS peaks centered at binding energies of 529.8 and 532.0 eV. The main peak at 532.0 eV has been assigned for O_2^{2-} and O^- ion deficiencies in the subsurface layer of metal oxides due to the formation of $Ce_{0.75}Zr_{0.25}O_2$ solid solution, $Ce_{0.90}Cu_{0.10}O_2$ solid solution and $Ce_{0.85}Ni_{0.15}O_2$ solid solution.[40–42] From Fig. 4, we also can see that the other peak at 529.8 eV has been assigned to the lattice oxygen in $Ce_{0.75}Zr_{0.25}O_2$, $Ce_{0.90}Cu_{0.10}O_2$ and $Ce_{0.85}Ni_{0.15}O_2$ (O^{2-} species). As shown in Table 1, the
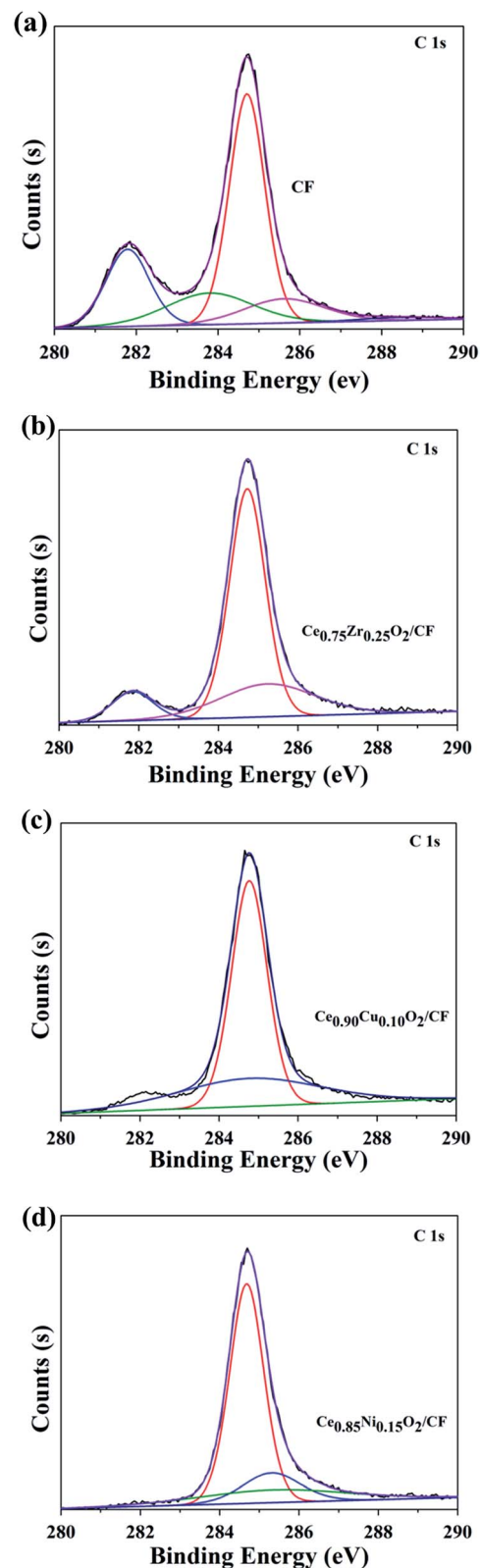
Fig. 3 C 1s spectra of CF (a), 2.0 wt% $Ce_{0.75}Zr_{0.25}O_2$/CF composite (b), 2.5 wt% $Ce_{0.90}Cu_{0.10}O_2$/CF composite (c) and 0.45 wt% $Ce_{0.85}Ni_{0.15}O_2$/CF composite (d).
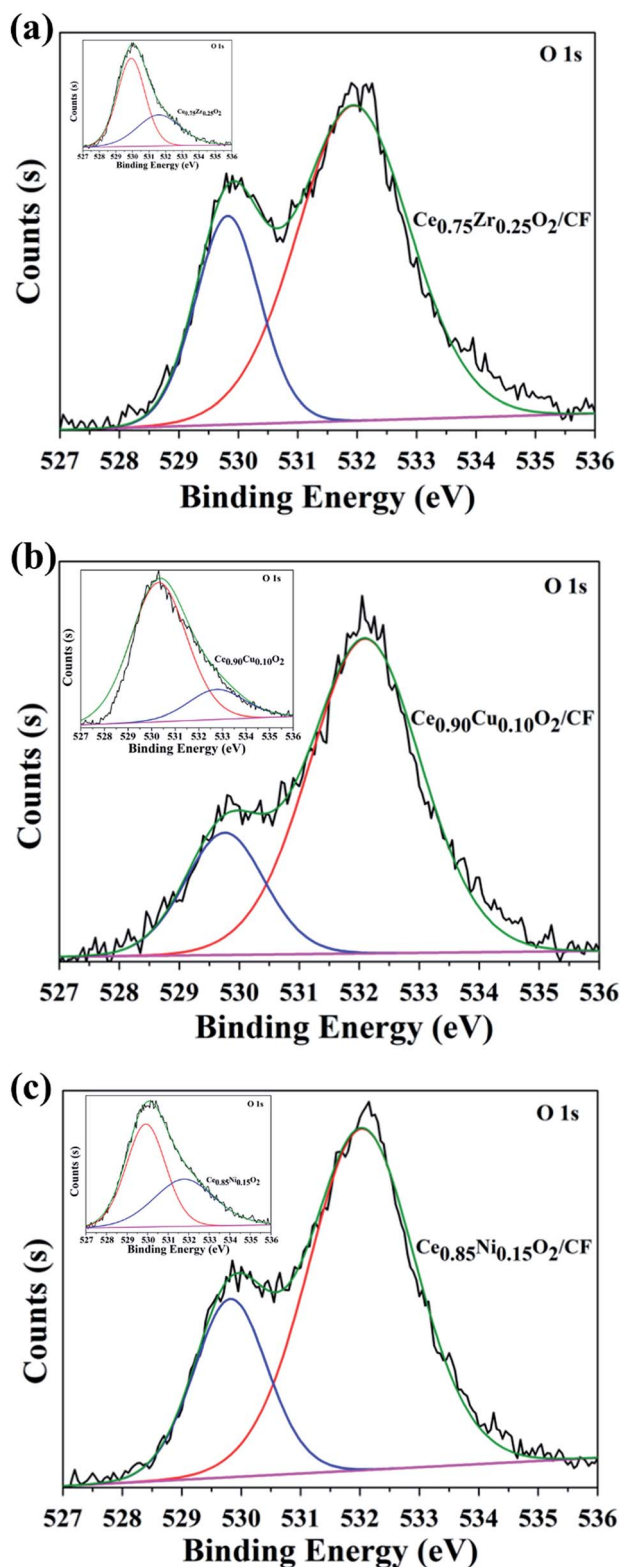
Fig. 4 O 1s spectra of 2.0 wt% $Ce_{0.75}Zr_{0.25}O_2$/CF composite (a), 2.5 wt% $Ce_{0.90}Cu_{0.10}O_2$/CF composite (b) and 0.45 wt% $Ce_{0.85}Ni_{0.15}O_2$/CF composite (c), the inserts in (a), (b) and (c) are O 1s spectra of $Ce_{0.75}Zr_{0.25}O_2$ composite, $Ce_{0.90}Cu_{0.10}O_2$ composite and $Ce_{0.85}Ni_{0.15}O_2$ composite, respectively.

Table 1 XPS analysis results of $Ce_xA_{1-x}O_2$ composite and $Ce_xA_{1-x}O_2$/CF composite

Cathode material	O_{ads}	O_{Latt}
$Ce_{0.75}Zr_{0.25}O_2$	17.64%	82.36%
$Ce_{0.90}Cu_{0.10}O_2$	41.50%	58.50%
$Ce_{0.85}Ni_{0.15}O_2$	35.80%	64.20%
$Ce_{0.75}Zr_{0.25}O_2$/CF	78.33%	21.67%
$Ce_{0.90}Cu_{0.10}O_2$/CF	72.50%	27.50%
$Ce_{0.85}Ni_{0.15}O_2$/CF	73.52%	26.48%

surface adsorption oxygen contents of $Ce_{0.75}Zr_{0.25}O_2$, $Ce_{0.90}Cu_{0.10}O_2$ and $Ce_{0.85}Ni_{0.15}O_2$ are 17.64%, 41.50% and 35.80%, respectively. And the surface lattice oxygen contents of $Ce_{0.75}Zr_{0.25}O_2$, $Ce_{0.90}Cu_{0.10}O_2$ and $Ce_{0.85}Ni_{0.15}O_2$ are 82.36%, 58.50% and 64.20%, respectively. However, when the $Ce_xA_{1-x}O_2$ composite is loaded on the CF, the surface adsorption oxygen contents of $Ce_{0.75}Zr_{0.25}O_2$/CF, $Ce_{0.90}Cu_{0.10}O_2$/CF and $Ce_{0.85}Ni_{0.15}O_2$/CF are 78.33%, 72.50% and 73.52%, respectively. And the surface lattice oxygen contents of $Ce_{0.75}Zr_{0.25}O_2$/CF, $Ce_{0.90}Cu_{0.10}O_2$/CF and $Ce_{0.85}Ni_{0.15}O_2$/CF are 21.67%, 27.50% and 26.48%, respectively. It is obvious that the surface adsorption oxygen contents of $Ce_xA_{1-x}O_2$/CF composite is more than that of $Ce_xA_{1-x}O_2$ composite. We can also see that $Ce_{0.90}Cu_{0.10}O_2$/CF and $Ce_{0.85}Ni_{0.15}O_2$/CF have similar adsorption oxygen and lattice oxygen contents. However, $Ce_{0.75}Zr_{0.25}O_2$/CF has higher adsorption oxygen content than that of other materials. The generation of rich adsorption oxygen can be mainly attributed to the formation of oxygen vacancies resulting from ZrO_2 cooperation into the CeO_2 lattice, which can provide superior conditions for the adsorption and activation of oxygen molecules and promote the formation of adsorption oxygen species on the surface of $Ce_{0.75}Zr_{0.25}O_2$ catalysts. The results of O 1s XPS analysis indicate that the existence of a large amount of adsorption oxygen on the catalyst surface can produce abundant active oxygen species that contributes to the high activity of the catalysts.

Fig. 5 shows XPS spectra of Ce 3d, Zr 3d, Cu 2p and Ni 2p for $Ce_xA_{1-x}O_2$/CF (A = Zr, Cu and Ni) composites, respectively. Fig. 5a corresponds to Ce 3d XPS spectra of the prepared samples at 875–925 eV. The Ce 3d XPS spectra exhibits eight obvious XPS peaks at binding energies of about 882.4, 884.3, 887.7, 898.6, 901.5, 903.4, 905.8, and 916.8 eV. The four main $3d_{5/2}$ features at 882.4, 884.3, 887.7, and 898.6 eV correspond to V, V_1, V_2 and V_3 components, while the $3d_{3/2}$ features at 901.3, 903.4, 905.8, and 916.8 eV correspond to U, U_1, U_2 and U_3 components, respectively.[43] The presence of the fingerprint U_3 satellite peak at about 916.8 eV confirms the Ce^{4+} oxidation state. The appearance of characteristic bands of Ce^{3+} labeled V_1 at 884.3 eV and U_1 at 903.5 eV suggests that both oxidation states Ce^{4+} and Ce^{3+} co-exist on the surfaces of $Ce_xA_{1-x}O_2$/CF composites. As shown in Fig. 5b, the two peaks approximately at 182.5 eV and 184.9 eV correspond to the Zr $3d_{5/2}$ and $3d_{3/2}$ spin–orbit states, respectively.[44] Fig. 5c presents the Cu 2p XPS spectra of $Ce_{0.90}Cu_{0.10}O_2$/CF composite. Three prominent XPS peaks can be observed at binding energies of 934.3, 941.5 and
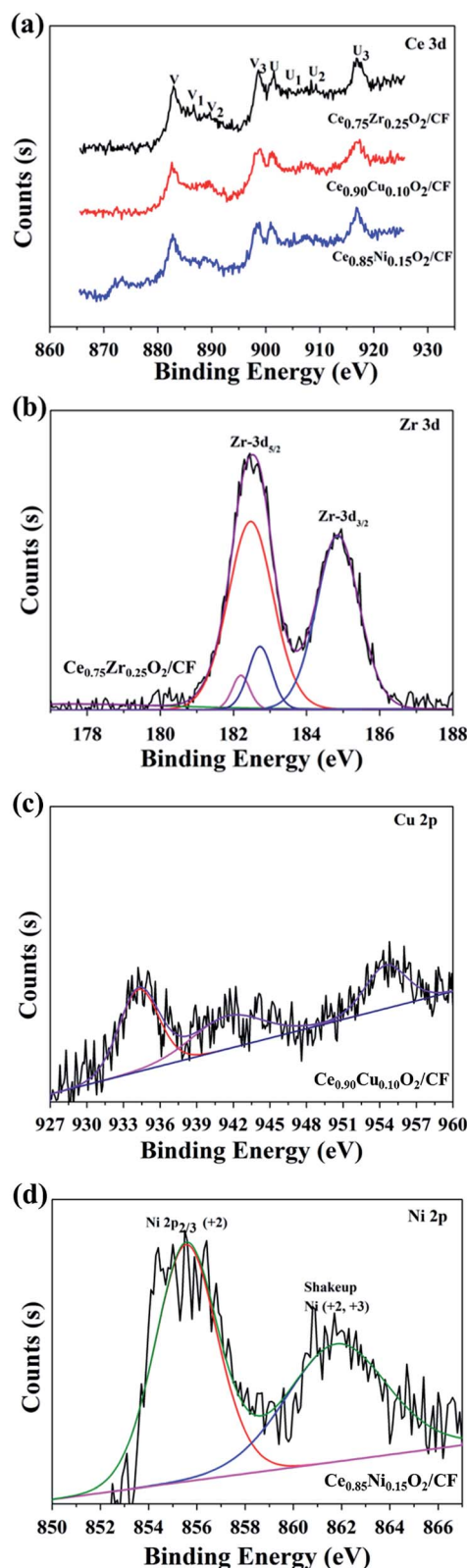
Fig. 5 XPS spectra of Ce 3d for $Ce_xA_{1-x}O_2$/CF (A = Zr, Cu and Ni) composites (a), Zr 3d for 2.0 wt% $Ce_{0.75}Zr_{0.25}O_2$/CF composite (b), Cu 2p for 2.5 wt% $Ce_{0.90}Cu_{0.10}O_2$/CF composite (c) and Ni 2p for 0.45 wt% $Ce_{0.85}Ni_{0.15}O_2$/CF composite (d).

954.5 eV, respectively. The XPS peaks centered at 934.3 and 954.5 eV correspond to Cu $2p_{3/2}$ and Cu $2p_{1/2}$, respectively. The peak at 941.5 is satellites arising from Cu $2p_{1/2}$. The satellite centered at about 939–944 eV and at a high Cu $2p_{3/2}$ binding Cu^{2+} content on the surface of the catalysts.[45] Fig. 5d shows Ni $2p_{3/2}$ for the $Ce_{0.85}Ni_{0.15}O_2$/CF composite. The main peak centered at 855.6 eV assigns to Ni^{2+} species. In addition, a broad peak at 861.8 eV is assigned as the shake-up satellite peak of Ni^{2+} (NiO) and Ni^{3+} (Ni_2O_3).[46]

To further identify the accurate element composition, the XPS wide scan spectra in the binding energy range of 0–1200 eV was performed on CF, 2.0 wt% $Ce_{0.75}Zr_{0.25}O_2$/CF composite, 2.5 wt% $Ce_{0.90}Cu_{0.10}O_2$/CF composite and 0.45 wt% $Ce_{0.85}Ni_{0.15}O_2$/CF composite as shown in Fig. S1.† As shown in Fig. S1,† it can be found that $Ce_{0.75}Zr_{0.25}O_2$, $Ce_{0.90}Cu_{0.10}O_2$ and $Ce_{0.85}Ni_{0.15}O_2$ nanoparticles successfully loaded on CF, respectively. And the atomic oxygen content on the surface increases with $Ce_xA_{1-x}O_2$ (A = Zr, Cu and Ni) composite load on CF (from 8.24% for CF to 13.49%, 12.71% and 13.15% for $Ce_{0.75}Zr_{0.25}O_2$/CF, $Ce_{0.90}Cu_{0.10}O_2$/CF and $Ce_{0.85}Ni_{0.15}O_2$/CF composite). Moreover, it revealed that the doping of Zr, Cu and Ni elements can improve the catalytic properties of CeO_2.

3.1.4 CV and EIS analysis. The electrochemical performance of the working electrode used for the CV and EIS tests is shown in Fig. 6. CV curves of $Ce_xA_{1-x}O_2$ (A = Zr, Cu and Ni) composite, $Ce_xA_{1-x}O_2$/CF composite and CF electrodes at a scan rate of 0.04 V s^{-1} in 50 mg L^{-1} CIP with 0.1 mmol L^{-1} Fe^{2+} and 0.05 mol L^{-1} Na_2SO_4 at pH = 3 solution are compared in Fig. 6a. We can see that the redox peak current values of $Ce_xA_{1-x}O_2$/CF (A = Zr, Cu and Ni) composite and CF electrodes are three orders of magnitude higher than that of $Ce_xA_{1-x}O_2$ composite. When $Ce_xA_{1-x}O_2$/CF (A = Zr, Cu and Ni) composite and CF are respectively used as cathodes, it is obvious that it is a typical irreversible process. The cathodic peak current density of CF is 0.0858 mA cm^{-2}, while those of $Ce_{0.75}Zr_{0.25}O_2$/CF, $Ce_{0.90}Cu_{0.10}O_2$/CF and $Ce_{0.85}Ni_{0.15}O_2$/CF increases to 0.1082, 0.1234 and 0.0863 mA cm^{-2}, respectively. It can be seen that the electric conductivity of $Ce_{0.75}Zr_{0.25}O_2$/CF, $Ce_{0.90}Cu_{0.10}O_2$/CF and $Ce_{0.85}Ni_{0.15}O_2$/CF is better than that of CF. Due to the higher peak current density, $Ce_{0.90}Cu_{0.10}O_2$/CF displays the best electrochemical activity. But the difference of the peak current density for these three electrodes is very small. To further investigate the reaction kinetics, the relationship between the peak current and the square root of scan rate is demonstrated in Fig. S2.† As shown in Fig. S2,† the peak current in 50 mg L^{-1} CIP with 0.1 mmol L^{-1} Fe^{2+} and 0.05 mol L^{-1} Na_2SO_4 at pH = 3 solution is proved to be linear variation with the change of the square root of scan rate. It reveals that the electrochemical behavior for all electrodes is controlled by diffusion process. And the higher slope value indicates a faster diffusion process.[33] Fig. S2† shows that $Ce_{0.90}Cu_{0.10}O_2$/CF exhibits the best electrochemical activity in 50 mg L^{-1} CIP with 0.1 mmol L^{-1} Fe^{2+} and 0.05 mol L^{-1} Na_2SO_4 at pH = 3 solution. However, the CIP degradation efficiency of $Ce_{0.90}Cu_{0.10}O_2$/CF composite as cathode is smaller than that of $Ce_{0.75}Zr_{0.25}O_2$/CF and $Ce_{0.85}Ni_{0.15}O_2$/CF, which demonstrates the electrochemical
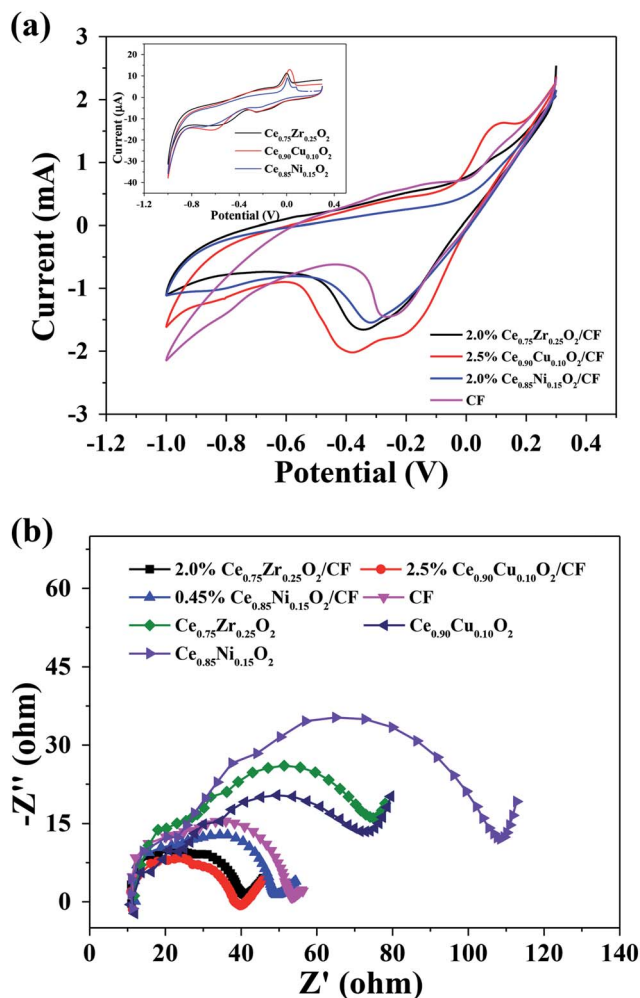
Fig. 6 (a) Cyclic voltammetry of $Ce_xA_{1-x}O_2$ (A = Zr, Cu and Ni) composite, $Ce_xA_{1-x}O_2$/CF composite and CF electrodes in 50 mg L^{-1} CIP with 0.1 mmol L^{-1} Fe^{2+} and 0.05 mol L^{-1} Na$_2$SO$_4$ at pH = 3 solution, the scan rate was 0.04 V s^{-1}, all scans were performed from the negative potential to positive potential and the initial potential was −1.0 V. (b) Nyquist plots of $Ce_xA_{1-x}O_2$ (A = Zr, Cu and Ni) composite, $Ce_xA_{1-x}O_2$/CF composite and CF electrodes under a potential of 0.8 V in 50 mg L^{-1} CIP with 0.1 mmol L^{-1} Fe^{2+} and 0.05 mol L^{-1} Na$_2$SO$_4$ at pH = 3 solution.

behaviors of $Ce_xA_{1-x}O_2$/CF composites are not the main factor to degrade CIP solution.

Fig. 6b shows the Nyquist plots of $Ce_xA_{1-x}O_2$ (A = Zr, Cu and Ni) composite, $Ce_xA_{1-x}O_2$/CF composite and CF electrodes under a potential of 0.8 V in 50 mg L^{-1} CIP with 0.1 mmol L^{-1} Fe^{2+} and 0.05 mol L^{-1} Na$_2$SO$_4$ at pH = 3 solution. It can be found that there is a semicircular part at high frequency which represents the charge transfer process. And the smaller of the radius of the semicircle, the better electrochemical activity of electrode and the faster of electron transfer rate. It can be seen that the electrochemical performance of CF is much better than that of $Ce_{0.75}Zr_{0.25}O_2$, $Ce_{0.90}Cu_{0.10}O_2$ and $Ce_{0.85}Ni_{0.15}O_2$. And the electrochemical performance of 2.0 wt% $Ce_{0.75}Zr_{0.25}O_2$/CF, 2.5 wt% $Ce_{0.90}Cu_{0.10}O_2$/CF and 0.45 wt% $Ce_{0.85}Ni_{0.15}O_2$/CF is better than that of CF. This is because $Ce_{0.75}Zr_{0.25}O_2$, $Ce_{0.90}Cu_{0.10}O_2$,

and $Ce_{0.85}Ni_{0.15}O_2$ nanoparticles are well dispersed on CF, respectively. And $Ce_{0.90}Cu_{0.10}O_2$/CF has the best electrochemical behavior. However, the difference of the semicircle radius for these three electrodes is very small.

3.2 Analysis of influence factors on the oxidative degradation of CIP

3.2.1 Effect of electric field on the degradation of CIP. To evaluate the feasibility of CF, $Ce_{0.75}Zr_{0.25}O_2$/CF, $Ce_{0.90}Cu_{0.10}O_2$/CF and $Ce_{0.85}Ni_{0.15}O_2$/CF cathodes in EF system, the performance of CIP degradation by the electro-Fenton, electrocatalysis and electrosorption effects are tested as a ref. 47.

Fig. 7 shows that CIP is rapidly degraded by electro-Fenton with CIP degradation efficiency of 83.03%, 100%, 93.07% and 95.90% after 1 h by using CF, $Ce_{0.75}Zr_{0.25}O_2$/CF, $Ce_{0.90}Cu_{0.10}O_2$/CF and $Ce_{0.85}Ni_{0.15}O_2$/CF, respectively. As shown in Fig. 7a, the degradation efficiency is 88.91% for electrosorption of CIP on CF (no Fe^{2+} and no $Ce_xA_{1-x}O_2$ adding) after 2 h which shows CF has a strong electrosorption behavior. The reason why there is a strong electrosorption behavior is that the carbon felt has large specific surface area and can produce 0.7054 mg L^{-1} H$_2$O$_2$ as a cathode after 2 h (from Fig. S4†). From Fig. 7b–d, we can see the degradation efficiency is respectively 96.24%, 92.64% and 95.75% for electrocatalysis and electrosorption of CIP by using the $Ce_{0.75}Zr_{025}O_2$/CF, $Ce_{0.90}Cu_{0.10}O_2$/CF and $Ce_{0.85}Ni_{0.15}O_2$/CF electrodes (no Fe^{2+} adding) which shows $Ce_xA_{1-x}O_2$ has a strong catalytic activity. The result is that 0.4235 mg L^{-1}, 0.3748 mg L^{-1} and 0.3980 mg L^{-1} H$_2$O$_2$ are produced when $Ce_{0.75}Zr_{0.25}O_2$/CF, $Ce_{0.90}Cu_{0.10}O_2$/CF and $Ce_{0.85}Ni_{0.15}O_2$/CF electrodes are individually used as cathode. And what's more, a Fenton-like reaction between Ce^{3+} and H$_2$O$_2$ may be happened. Therefore, synergistic effects from the predominant role of the Fenton reaction of Fe^{2+} and H$_2$O$_2$ forming homogeneous ·OH and the Fenton-like reaction of Ce^{3+} and H$_2$O$_2$ producing heterogeneous ·OH and the electrocatalytic activity of $Ce_xA_{1-x}O_2$ (A = Zr, Cu and Ni) composites and the strong adsorption of CF contribute to the degradation efficiency of CIP in electro-Fenton system.

3.2.2 Effect of $Ce_xA_{1-x}O_2$/CF composites (A = Zr, Cu and Ni) with different ratios of Ce and A on the degradation efficiency of CIP. To confirm the optimal constitution of the $Ce_xA_{1-x}O_2$/CF composites (A = Zr, Cu and Ni), quality ratios of Ce/A were investigated through the degradation efficiency for CIP at the experiment condition of 400 mA, pH = 3 and 0.1 mmol L^{-1} Fe^{2+} solution.

From Fig. 8a, it can be seen that with the increase of Zr doping amount, the CIP degradation efficiency increased and then decreased when the load capacity of $Ce_{1-x}Zr_xO_2$ (the Zr loading, x wt%) was fixed at 2.0 wt%. The degradation efficiencies of CIP for Ce/Zr quality ratio of 0.85 : 0.15, 0.75 : 0.25 and 0.65 : 0.35 were 94.78%, 100% and 92.66% after 2 h, respectively. So the Ce/Zr ratio of 0.75 : 0.25 exhibited the highest degradation efficiency, which demonstrates $Ce_{0.75}Zr_{0.25}O_2$ composite having a large amount of oxygen vacancy and strong electrocatalytic activity. As shown in Fig. 8b, it was found that the degradation efficiency for CIP increased first and then decreased with the increase of the Cu doping
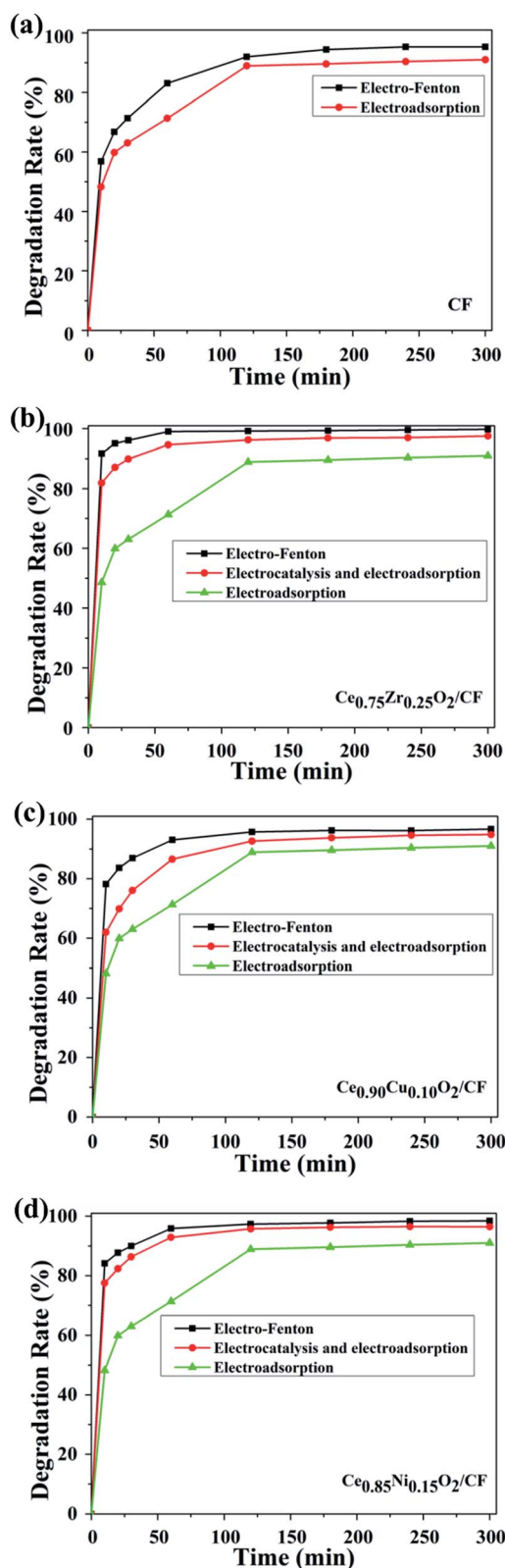
Fig. 7 Degradation efficiency of CIP by electro-Fenton, electro-catalysis and electrosorption (a) CF, (b) $Ce_{0.75}Zr_{0.25}O_2/CF$, (c) $Ce_{0.90}Cu_{0.10}O_2/CF$, (d) $Ce_{0.85}Ni_{0.15}O_2/CF$ at the experiment condition: pH = 3, 0.1 mmol L^{-1} Fe^{2+} and 0.05 mol L^{-1} Na_2SO_4 solution.
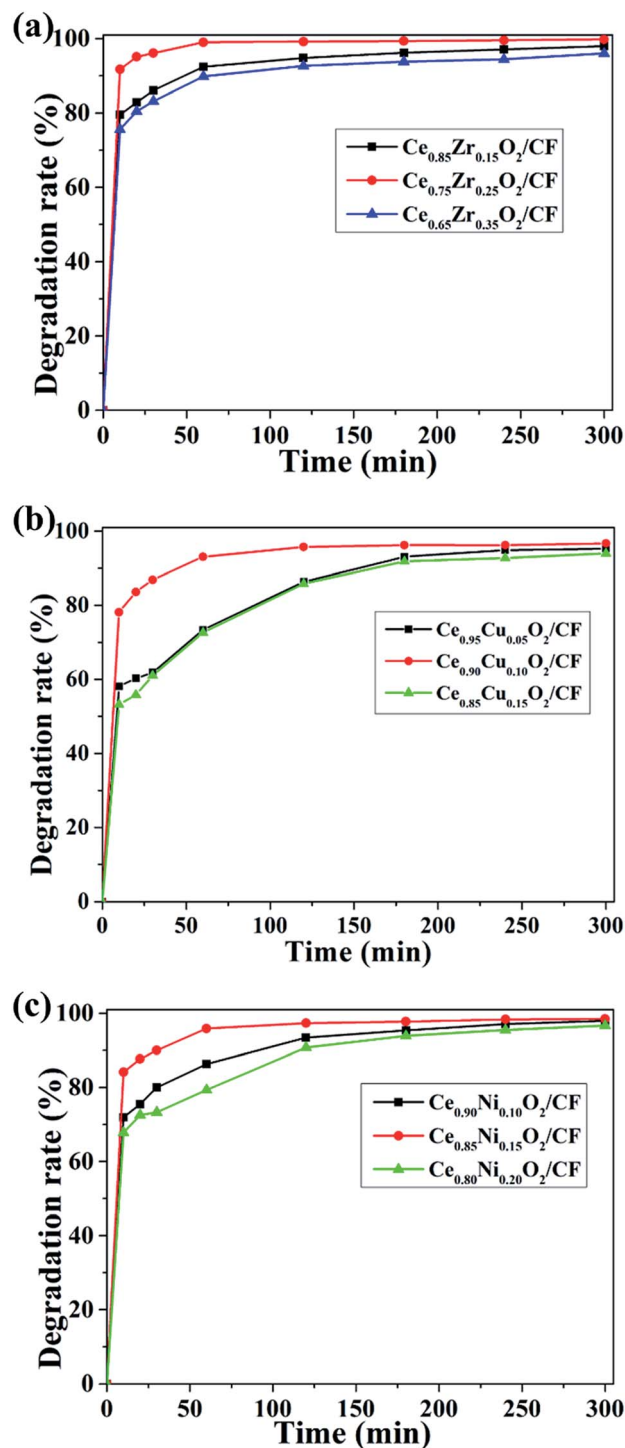

Fig. 8 Degradation efficiency of CIP in the presence of $Ce_xA_{1-x}O_2/CF$ composites (A = Cu and Ni) with different Ce/Zr (a), Ce/Cu (b) and Ce/Ni ratios (c) at the experiment condition: pH = 3, 0.1 mmol L^{-1} Fe^{2+} and 0.05 mol L^{-1} Na_2SO_4 solution.

amount when the load capacity of $Ce_{1-x}Cu_xO_2$ (the Cu loading, x wt%) was fixed at 2.5 wt%. The CIP degradation efficiencies of CIP for Ce/Cu quality ratio of 0.95 : 0.05, 0.90 : 0.10 and 0.85 : 0.15 were 86.35%, 95.70% and 87.84% after 2 h, respectively. So the Ce/Cu ratio of 0.90 : 0.10 exhibited the highest

degradation efficiency, which indicates $Ce_{0.90}Cu_{0.10}O_2$ composite has a large amount of oxygen vacancy and strong electrocatalysis effect. When $Ce_{1-x}Ni_xO_2$ (the Ni loading, x wt%) load capacity was fixed at 0.45 wt%, it could be seen that the CIP degradation efficiency also increased first and then decreased with increase of the Ni doping amount from Fig. 8c. The CIP degradation efficiencies of CIP for Ce/Ni quality ratio of 0.80 : 0.20, 0.85 : 0.15 and 0.90 : 0.10 were 90.77%, 97.33% and 93.40% after 2 h, respectively. Apparently, the Ce/Ni ratio of 0.85 : 0.15 exhibited the highest degradation efficiency which showed $Ce_{0.85}Ni_{0.15}O_2$ composite having large amount of oxygen vacancy and strong electrocatalytic activity.

3.2.3 Effect of $Ce_xA_{1-x}O_2$ loading capacity on the degradation of CIP.
To research the effect of $Ce_xA_{1-x}O_2$ loading on the decay of CIP, we chose the $Ce_{0.75}Zr_{0.25}O_2$/CF and $Ce_{0.90}Cu_{0.10}O_2$/CF and $Ce_{0.85}Ni_{0.15}O_2$/CF composite as cathodes to degrade CIP at 400 mA and pH = 3, respectively. It was shown in Fig. 9 that the degradation of CIP was dependent strongly on the loading quantity of $Ce_xA_{1-x}O_2$ (A = Zr, Cu, Ni).

As shown in Fig. 9a, there was a positive effect on CIP degradation when $Ce_{0.75}Zr_{0.25}O_2$ load increased from 1.0 wt% to 2.0 wt%. Meanwhile, the CIP solution degradation efficiency increased from 96.02% to 100% after 1 h. This effect might be due to the increase of oxygen vacancies with the increase of $Ce_{0.75}Zr_{0.25}O_2$ loading. Thus, more $\cdot$OH could be formed by $Ce_{0.75}Zr_{0.25}O_2$ and Fe^{2+} catalysis. That is to say, there is a synergy between Fe^{2+} and Ce^{3+} to make feasible a larger production of hydroxyl radical.[32] However, with the further increase of $Ce_{0.75}Zr_{0.25}O_2$ loading, the degradation efficiency decreased to 94.54% and 94.24% for 2.5 wt% and 3.0 wt% $Ce_{0.75}Zr_{0.25}O_2$ loading, respectively. It may be due to the too much loading of $Ce_{0.75}Zr_{0.25}O_2$, so that the conductivity of $Ce_{0.75}Zr_{0.25}O_2$/CF electrode became poor.

Fig. 9b shows the influence of different loading capacity of $Ce_{0.90}Cu_{0.10}O_2$ on the degradation of the CIP. When $Ce_{0.90}Cu_{0.10}O_2$ loading increased from 1.0 wt% to 2.5 wt% on the CF, we found that the degradation efficiency of CIP increased from 86.86% to 93.07% after 2 h. However, the degradation efficiency of CIP of 2.5 wt% $Ce_{0.90}Cu_{0.10}O_2$ loading on CF only reached 96.65% after 5 h. This may be caused by the adsorption of a large number of CIP intermediates on the surface of $Ce_{0.90}Cu_{0.10}O_2$, which affected production of oxygen vacancy and the electro-conductivity of $Ce_{0.90}Cu_{0.10}O_2$/CF electrode. It could be seen that the removal rate of CIP decreased to 87.08% of 3.0 wt% $Ce_{0.90}Cu_{0.10}O_2$ loading from Fig. 9b. Because $Ce_{0.90}Cu_{0.10}O_2$ content was too high in $Ce_{0.90}Cu_{0.10}O_2$/CF composite which led to blocking the pores of $Ce_{0.90}Cu_{0.10}O_2$/CF composite, and then the effective area for O_2 adsorption decreased which contributed to producing less oxygen vacancy.

From Fig. 9c, we could see that the CIP degradation efficiency increased from 87.59% to 95.90% after 1 h with the increase of $Ce_{0.85}Ni_{0.15}O_2$ loading from 0.14 wt% to 0.45 wt% on CF, respectively. And the CIP degradation efficiency of 0.45 wt% $Ce_{0.85}Ni_{0.15}O_2$ loading on CF reached to 98.33% after 4 h. That maybe that more oxygen vacancies were produced when the loading of $Ce_{0.85}Ni_{0.15}O_2$ increased and more $\cdot$OH was
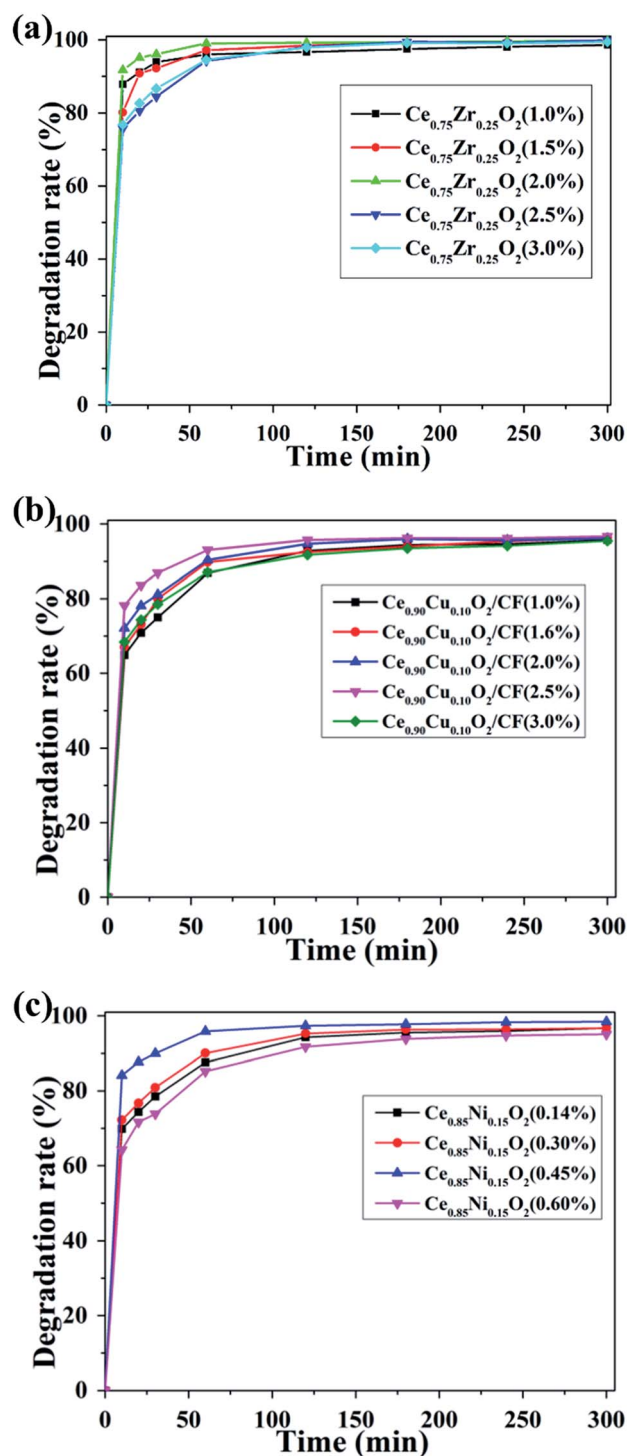
Fig. 9 Effect of (a) $Ce_{0.75}Zr_{0.25}O_2$, (b) $Ce_{0.90}Cu_{0.10}O_2$, (c) $Ce_{0.85}Ni_{0.15}O_2$ load capacity on degradation efficiency of CIP at pH = 3, 400 mA, 0.1 mmol L^{-1} Fe^{2+} and 0.05 mol L^{-1} Na_2SO_4 solution of the experiment condition.

produced. However, when the $Ce_{0.85}Ni_{0.15}O_2$ loading increased to 0.6 wt%, the CIP solution removal rate reached 85.23% and 94.75% after 1 h and 4 h, respectively. That was because the conductivity of $Ce_{0.85}Ni_{0.15}O_2$/CF electrode became poor.

Overall, Fig. 9 shows the optimal load capacity of $Ce_{0.75}Zr_{0.25}O_2$, $Ce_{0.90}Cu_{0.10}O_2$ and $Ce_{0.85}Ni_{0.15}O_2$ on CF was 2.0 wt%, 2.5 wt% and 0.45 wt%, respectively. And their corresponding CIP degradation efficiencies were about 100%, 93.07% and 95.9% at 1 h, respectively. The highest degradation performance was measured for the $Ce_{0.75}Zr_{0.25}O_2$/CF electrode at the experiment condition of 400 mA, pH = 3, 0.1 mmol L^{-1} Fe^{2+} and 0.05 mol L^{-1} Na_2SO_4 solution.

3.2.4 Effect of applied current on the degradation of CIP.

The formation rate of H_2O_2 is crucial for the oxidative degradation of organic pollutants in EF process. And the optimal generation rate of H_2O_2 depends on the applied current, which increases with the increasing applied current.[48] However, continuous increase of the current can also decrease the generation of H_2O_2 because of the promotion of 4e reduction of O_2 leading to the formation of H_2O as side reaction.[14] Therefore, the applied current is a main parameter in EF process. And it affects the electro-catalytic activity of the circulation of Ce^{4+} and Ce^{3+}.[49]

Fig. 10a shows the effect of applied current on the oxidative degradation of CIP by using CF as cathode. The degradation efficiency increases from 61.84% to 83.03% after 1 h when the applied current increased from 100 to 400 mA. This enhanced degradation efficiency of CIP is due to higher electrochemical production of H_2O_2 and Fe^{2+} catalyst regeneration causing a higher concentration of homogeneous ·OH in the solution. In addition, the increased current density leads to an enhanced production of Pt (·OH) on the anode surface.[18] However, further increase in current to 500 mA, the CIP degradation efficiency reaches 81.87% after 1 h which is lower than that of 400 mA. This is because the side reactions have an enhanced rate which competes with the CIP oxidative degradation.[50] The main side reactions as follows:

$$O_2 + 4e^- + H^+ = H_2O \tag{1}$$

$$H_2O + 2e^- = H_2 + 2OH^- \tag{2}$$

$$H_2O_2 = O_2 + 2H^+ + 2e^- \tag{3}$$
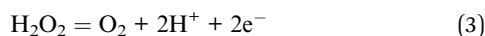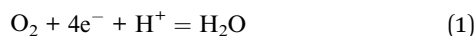
Therefore, 400 mA is the optimal current value on the CIP degradation.

As shown in Fig. 10b, the oxidation degradation performance of the $Ce_{0.75}Zr_{0.25}O_2$/CF composites as cathode is tested under the same operating conditions. Obtained results showed that the CIP degradation efficiency is accelerated from 87.87% to about 100% after 1 h by increasing the applied current from 100 to 400 mA. This is probably related to higher electrochemical production of H_2O_2 and Fe^{2+} catalyst regeneration and Ce^{3+} catalyst generation occurring at the $Ce_{0.75}Zr_{0.25}O_2$/gas interface[51] causing a higher concentration of ·OH. However, further increase current to 500 mA, the degradation efficiency of CIP decreases which can explained by acceleration of side reactions (eqn (1)–(3)) at higher current values. So the optimal current is 400 mA for the degradation of CIP when $Ce_{0.75}Zr_{0.25}O_2$/CF composites used as cathode.
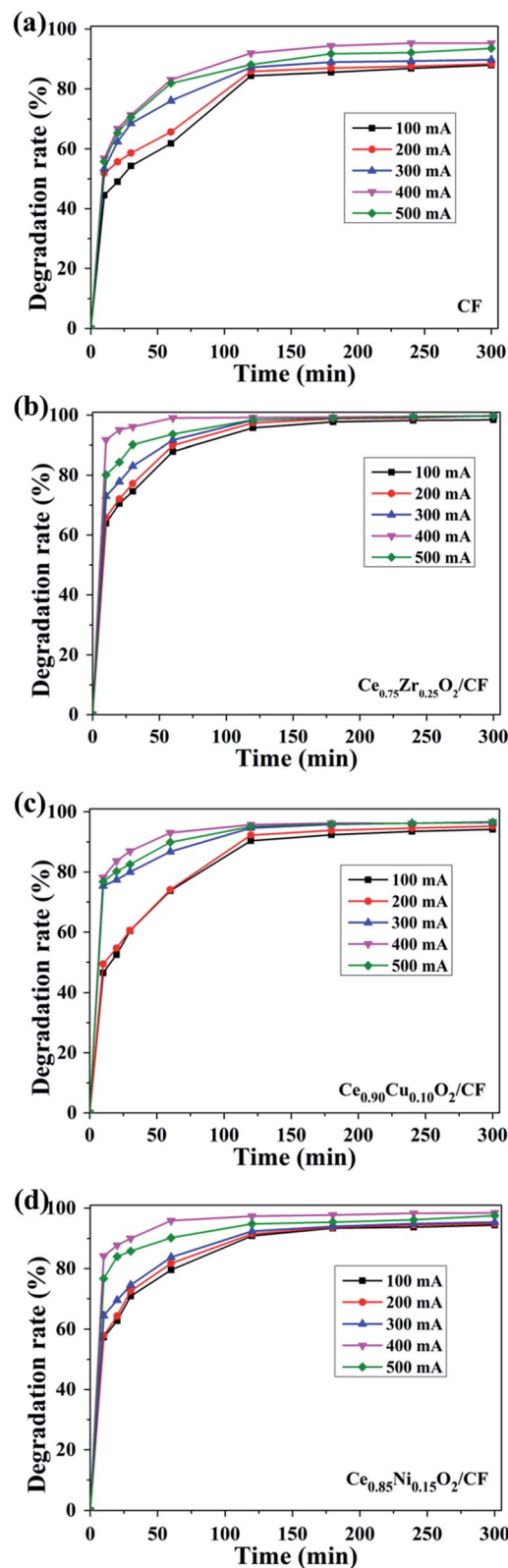

Fig. 10 Effect of applied current on the degradation of CIP in the cell of (a) Pt/CF, (b) Pt/$Ce_{0.75}Zr_{0.25}O_2$/CF, (c) Pt/$Ce_{0.90}Cu_{0.10}O_2$/CF, (d) Pt/$Ce_{0.85}Ni_{0.15}O_2$/CF experiment condition: pH = 3, 0.1 mmol L^{-1} Fe^{2+} and 0.05 mol L^{-1} Na_2SO_4 solution.

Fig. 10c shows the impact of different applied current on the decay of the CIP by using as $Ce_{0.90}Cu_{0.10}O_2$/CF as cathode in the EF process. Due to electrochemical production of H_2O_2 from O_2 reduction and the electro-catalysis of Fe^{2+} and Ce^{3+}, the degradation efficiency of CIP increases from 60.42% to 86.90% after 0.5 h electrolysis when the applied current increases from 100 to 400 mA. However, when the applied current is 500 mA, the degradation efficiency is reduced to 82.54% owing to fast occurrence of side reactions (eqn (1)–(3)). So the optimal current is 400 mA using as $Ce_{0.90}Cu_{0.10}O_2$/CF composite as cathode during the degradation of CIP.

The results obtained with Pt as anode and $Ce_{0.85}Ni_{0.15}O_2$/ CF as cathode are depicted in Fig. 10d. The CIP degradation efficiency increases from 79.54% to 95.9% after 1 h when the applied current increases from 100 to 400 mA. The results show that the higher the applied current, the higher the decay in CIP concentration. This is because in addition to higher electrochemical production of H_2O_2 and Fe^{2+} catalyst regeneration, as well as the circle of Ce^{4+}/Ce^{3+} which leads to produce a large number of ˙OH. And it further brings about the formation of H_2O_2 from O_2 reduction. However, the degradation efficiency decreases to 95.90% under the applied current of 500 mA owing to side reactions occurrence (eqn (1)–(3)).

Overall, the optimal current is 400 mA during the degradation of CIP for different electrodes. Due to the electrocatalysis of $Ce_{0.75}Zr_{0.25}O_2$ composite, $Ce_{0.90}Cu_{0.10}O_2$ composite and $Ce_{0.85}Ni_{0.15}O_2$ composite, the CIP degradation efficiency by using CF as cathode is lower than that of $Ce_{0.75}Zr_{0.25}O_2$/CF composite, $Ce_{0.90}Cu_{0.10}O_2$/CF composite and $Ce_{0.85}Ni_{0.15}O_2$/CF composite as cathode, respectively. And the degradation efficiency of $Ce_{0.75}Zr_{0.25}O_2$/CF composite as cathode is higher than that of $Ce_{0.85}Ni_{0.15}O_2$/CF composite and $Ce_{0.90}Cu_{0.10}O_2$/CF composite as cathodes. This is because $Ce_{0.75}Zr_{0.25}O_2$ composites have larger specific surface area, that is to say, it has a more catalytic active sites, than $Ce_{0.90}Cu_{0.10}O_2$ composite and $Ce_{0.85}Ni_{0.15}O_2$ composite which results in producing a small amount of oxygen vacancies.

To compare specific surface area and pore volume of $Ce_{0.75}Zr_{0.25}O_2$ and $Ce_{0.90}Cu_{0.10}O_2$ and $Ce_{0.85}Ni_{0.15}O_2$ nanoparticles, the N_2 adsorption–desorption was performed. As shown in Fig. S3a,† bimodal pore size distribution was found in $Ce_{0.75}Zr_{0.25}O_2$ material with average pore diameters of ~34 nm which was larger than that of $Ce_{0.90}Cu_{0.10}O_2$ and $Ce_{0.85}Ni_{0.15}O_2$ materials (Fig. S3b†). In addition, the obtained pore volumes for $Ce_{0.75}Zr_{0.25}O_2$ and $Ce_{0.90}Cu_{0.10}O_2$ and $Ce_{0.85}Ni_{0.15}O_2$ materials are ~0.15 and 0.079 and 0.13 cm^3 g^{-1}, respectively (Table S1†). It was found that the $Ce_{0.75}Zr_{0.25}O_2$ material exhibits a higher BET surface area compared to that of $Ce_{0.90}Cu_{0.10}O_2$ and $Ce_{0.85}Ni_{0.15}O_2$ materials (Table S1†). Overall, this observation indicates $Ce_{0.75}Zr_{0.25}O_2$ nanoparticles had lager specific surface area and pore volume than $Ce_{0.90}Cu_{0.10}O_2$ and $Ce_{0.85}Ni_{0.15}O_2$ nanoparticles which caused more flexible response to the active site so that producing more oxygen vacancies. And further it could produce a larger number of H_2O_2 by oxygen reduction which contributed to the degradation of CIP.

3.3 Comparison of degradation and mineralization efficiency of CIP aqueous solution

It is crucial to completely remove organic pollutants from wastewater. The EF process can degrade and mineralize the organic matter in aqueous solution and further achieve high CIP degradation and TOC removal efficiency. Furthermore, the degradation efficiency and mineralization degree of this technology depend on several parameters, one of the most crucial is the nature of the cathode material used.

The degradation of CIP solution was carried out by using different modified cathodes ($Ce_{0.75}Zr_{0.25}O_2$/CF, $Ce_{0.90}Cu_{0.10}O_2$/ CF, $Ce_{0.85}Ni_{0.15}O_2$/CF) at 400 mA and pH = 3. Fig. 11a showed that the CIP solution degradation efficiency of 2.0 wt% $Ce_{0.75}Zr_{0.25}O_2$/CF reached about 100% after 1 h. The degradation efficiency of 2.5 wt% $Ce_{0.90}Cu_{0.10}O_2$/CF was much higher than that of CF before electrolysis of 2 h and even its electrolytic efficiency reached 93.07% after 1 h. But the degradation efficiency of $Ce_{0.90}Cu_{0.10}O_2$/CF and CF was about the same after 5 h. And the CIP solution degradation efficiency of 0.45 wt%

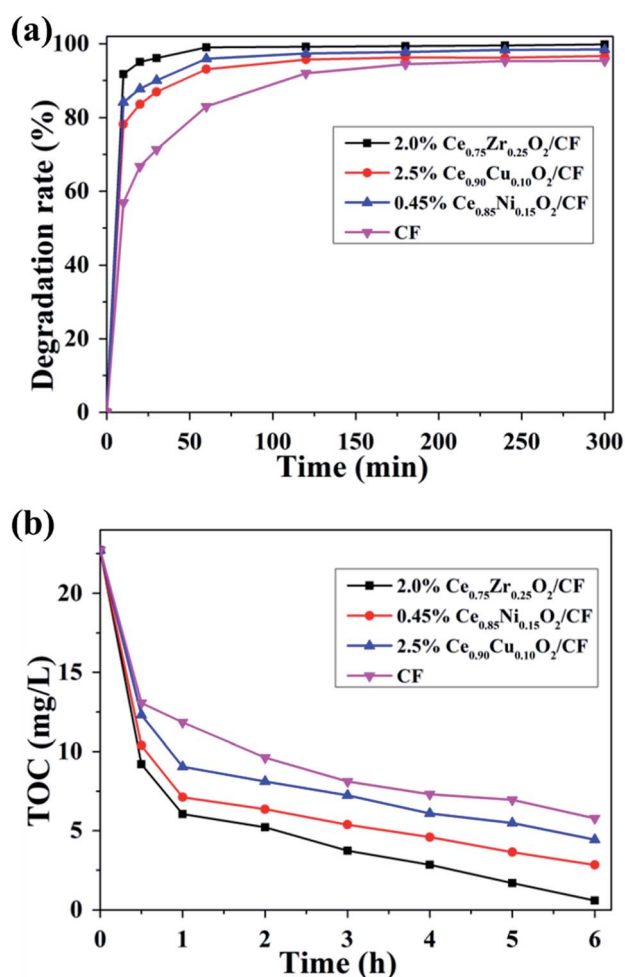**Fig. 11** Effect of $Ce_xA_{1-x}O_2$/CF (A = Zr, Cu and Ni) cathode on the degradation rate (a) and the extent of TOC removal (b) of CIP aqueous solution at pH = 3, 400 mA, 0.1 mmol L^{-1} Fe^{2+} and 0.05 mol L^{-1} Na_2SO_4 solution.

$Ce_{0.85}Ni_{0.15}O_2/CF$ attained 95.9% and 98.45% after 1 and 3 h, respectively. Further comparison of 2.0 wt% $Ce_{0.75}Zr_{0.25}O_2/CF$, 2.5 wt% $Ce_{0.90}Cu_{0.10}O_2/CF$ and 0.45 wt% $Ce_{0.85}Ni_{0.15}O_2/CF$ showed that 2.0 wt% $Ce_{0.75}Zr_{0.25}O_2/CF$ was the outstanding one. Although $Ce_{0.90}Cu_{0.10}O_2/CF$ has a greater electrical conductivity than $Ce_{0.75}Zr_{0.25}O_2/CF$ and $Ce_{0.85}Ni_{0.15}O_2/CF$, $Ce_{0.75}Zr_{0.25}O_2$ nanoparticles had lager specific surface area and pore volume than $Ce_{0.90}Cu_{0.10}O_2$ and $Ce_{0.85}Ni_{0.15}O_2$ nanoparticles (Table S1†) which resulted in having more catalytic activity sites to contribute to the entry of oxygen to obtain a higher concentration of hydrogen peroxide (Fig. S4†).

As it could be seen in Fig. 11b, the mineralization of CIP was improved by $Ce_xA_{1-x}O_2$ (A = Zr, Cu and Ni) loading on CF. When $Ce_{0.75}Zr_{0.25}O_2/CF$ was used as cathode in EF process, there was a maximum value of the TOC removal. Because $Ce_{0.75}Zr_{0.25}O_2$ nanoparticles had larger specific surface area (Table S1†) which led to having fast mass and electron transport rate. $Ce_{0.75}Zr_{0.25}O_2/CF$ composite had more catalytic activity sites than that of $Ce_{0.90}Cu_{0.10}O_2/CF$ composite and $Ce_{0.85}Ni_{0.15}O_2/CF$ composite. And $Ce_{0.75}Zr_{0.25}O_2/CF$ composite had more oxygen vacancies which resulted in the formation of H_2O_2 with higher concentration (Fig. S4†). From Fig. 11, the mineralization degree of CIP aqueous solution by using $Ce_{0.75}Zr_{0.25}O_2/CF$ during electro-Fenton system was 97.45% after 6 h owing to synergistic effects from the predominant role of homogeneous $^\cdot OH$ and the Fenton-like reaction of Ce^{3+} and H_2O_2 producing heterogeneous $^\cdot OH$ and the electrocatalytic activity of $Ce_xA_{1-x}O_2$ (A = Zr, Cu and Ni) composites and strong adsorption property of CF. It could be also found that removal rate of TOC was fast during the early treatment time, but it became slowly with the increase of time. The decrease of the mineralization rate was related to the formation of the precipitation of soluble iron species[52] and the consumption of $^\cdot OH$.[53]

It is well-known that the concentration of H_2O_2 is a very important parameter during CIP degradation in electro-Fenton process. Herein, the concentration of H_2O_2 is investigated by potassium iodide spectrophotometry ($\lambda = 352$ nm, $\varepsilon_{max} = 26\,400$ M^{-1} cm^{-1}). After applying current, the reduction reactions of Fe^{3+}/Fe^{2+} and Ce^{4+}/Ce^{3+} rapidly happen and more oxygen vacancies will be produced. And the Pt anode allows to generate supplementary hydroxyl radical from the oxidation of water on its surface.[54,55]

It can be seen that the H_2O_2 concentration sharply increases for the first 10 min from Fig. S4,† which is consistent with the results of Fig. 11. From Fig. 11, the CIP degradation efficiency and the mineralization degree also increase rapidly at this time. After 10 min, the H_2O_2 concentration decreases gradually, but it still remains the effective values and the degradation rate still increases at this time. This maybe because a large number of CIP intermediates adsorbed on the surface of $Ce_xA_{1-x}O_2$ and iron deposits and Fe(III)-carboxylate products adsorbed on CF which causes the decrease of the production of oxygen vacancy and the poor electrical conductivity. It can be also found that the concentration of H_2O_2 is lower for $Ce_xA_{1-x}O_2/CF$ (A = Zr, Cu and Ni) as cathodes than that of CF. Because the strong electrocatalysis of $Ce_xA_{1-x}O_2$ and a Fenton-like reaction of Ce^{3+} and H_2O_2 can consume a large amount of hydrogen peroxide. We

can find the amount of H_2O_2 produced by $Ce_{0.75}Zr_{0.25}O_2/CF$ as cathode is similar to that of CF as cathode at 5 h which indicates the catalytic action of $Ce_xA_{1-x}O_2$ composites plays a very important role in addition to the production of hydroxyl radicals. The production of H_2O_2 of $Ce_{0.90}Cu_{0.10}O_2/CF$ and $Ce_{0.85}Ni_{0.15}O_2/CF$ as cathodes is lower than that of $Ce_{0.75}Zr_{0.25}O_2/CF$ as cathode owing to the smaller specific surface area and pore volume of $Ce_{0.90}Cu_{0.10}O_2$ and $Ce_{0.85}Ni_{0.15}O_2$ nanoparticles (Table S1†) leading to producing small amount of H_2O_2. Above all, $Ce_{0.75}Zr_{0.25}O_2/CF$ electrode has a higher adsorption oxygen content than the other materials which can be mainly attributed to the formation of oxygen vacancies (Table 1).

3.4 Degradation mechanism of CIP

Samples withdrawn after 1 h in 0.05 mol L^{-1} Na_2SO_4 with 0.1 mmol L^{-1} Fe^{2+} at pH 3.0 using a $Pt/Ce_{0.75}Zr_{0.25}O_2/CF$ cell at 400 mA are analyzed by HPLC-MS. Apart from CIP, it can also be found that the name, molecular structure and m/z values of seven intermediates from Table S2.† These compounds are formed via hydroxylation, defluorination, cleavage of C–N bonds, deamination and breaking of the dihydroquinoline moiety. Since hydroxyl radicals are the main oxidizing agents in all the EAOPs tested, one can also expect the generation of the same intermediates in $Pt/Ce_{0.90}Cu_{0.10}O_2/CF$, $Pt/Ce_{0.85}Ni_{0.15}O_2/CF$ and Pt/CF cells. However, the intermediate of m/z (201) only can be found in the $Pt/Ce_{0.75}Zr_{0.25}O_2/CF$ cell.

Based on the products of Table S2† and literatures of the degradation mechanism of CIP,[56,57] a possible degradation path of CIP is proposed. As shown in Fig. 12, the path is initiated by the oxidation of CIP to generate either A via defluorination with hydroxylation or D by cleavage of two C–N bonds of the piperazinyl group. Further the hydroxylation of A yields B, whereas D produces E by the deamination. The cleavage of two C–N bonds of the piperazinyl group of B leads to producing C, nevertheless, F further is formed via the loss of the acetylene group of E. The loss of the lateral groups of compound F along with the breaking of the dihydroquinoline moiety yields G. C and G are further oxidized by $^\cdot OH$ to form short chain carboxylates which can ultimately produce CO_2, H_2O and inorganic ions owing to strong oxidizing property of $^\cdot OH$.

3.5 Stability of $Ce_{0.75}Zr_{0.25}O_2/CF$ cathode

Because the reuse performance of modified cathode is vital for industrial application, the stability of $Ce_{0.75}Zr_{0.25}O_2/CF$ cathode is tested 5 times after 60 min. As shown in Fig. 13, the
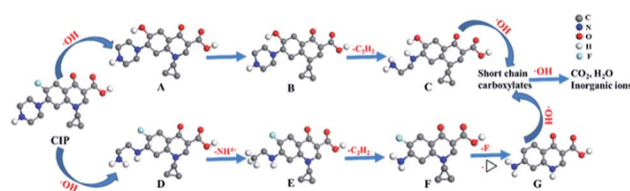

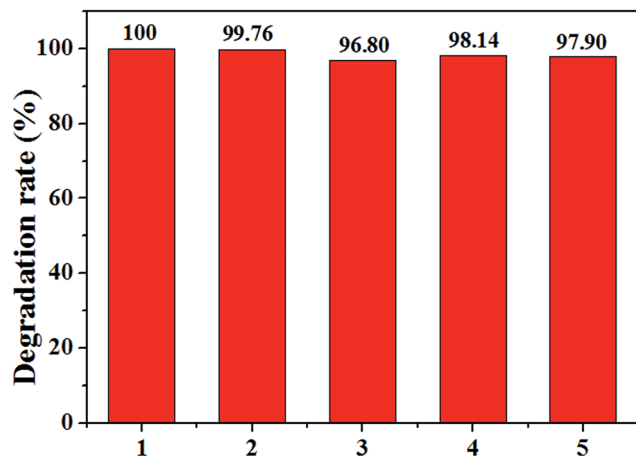Fig. 12 Proposed degradation pathways for CIP.

Fig. 13 The stability test of $Ce_{0.75}Zr_{0.25}O_2$/CF cathode in 5 times continuous runs in EF system at the experiment condition of 400 mA, pH = 3, 0.1 mmol L^{-1} Fe^{2+} and 0.05 mol L^{-1} Na$_2$SO$_4$ solution.

degradation efficiency of CIP is almost stable in all 5 runs. The CIP removal kept all above 97% except the third time with a slight decrease with a value of 96.80% at 60 min. According to the publication,[58–60] the standard deviation (SD) can also evaluate the repeatability or stability of different cathode materials. By calculating, we can see its value is between 0.12% and 1.6%. These results imply that the stability of cathodic material ensures good quality of waste water treatment after five runs in the electro-Fenton system at the experiment condition of 400 mA, pH = 3, 0.1 mmol L^{-1} Fe^{2+} and 0.05 mol L^{-1} Na$_2$SO$_4$ solution. That is to say, the $Ce_{0.75}Zr_{0.25}O_2$/CF cathode material has high stability and is suit to application in electro-Fenton system.

4   Conclusions

$Ce_xA_{1-x}O_2$/CF (A = Zr, Cu and Ni) composites were prepared successfully by impregnating CF into $Ce_xA_{1-x}O_2$ solid solution and then dried and calcined. Four different cathode materials ($Ce_{0.75}Zr_{0.25}O_2$/CF, $Ce_{0.90}Cu_{0.10}O_2$/CF, $Ce_{0.85}Ni_{0.15}O_2$/CF and CF) have been investigated for the degradation of CIP. About 100% degradation efficiency at 1 h and 97.45% mineralization efficiency (in terms of TOC removal) at 6 h were obtained with a $Ce_{0.75}Zr_{0.25}O_2$/CF cathode owing to synergistic effects from the predominant role of the Fenton reaction of Fe^{2+} and H$_2$O$_2$ forming homogeneous ˙OH and the Fenton-like reaction of Ce^{3+} and H$_2$O$_2$ producing heterogeneous ˙OH and the electro-catalytic activity of $Ce_{0.75}Zr_{0.25}O_2$ composite and the strong electrosorption of carbon felt. Eight intermediates were detected via HPLC-MS analysis. Based on them, a possible path of CIP degradation was proposed in the paper.

Acknowledgements

Notes and references

1 C. H. Huang, J. E. Renew, K. L. Smeby, K. Pinkston and D. L. Sedlak, *Water Res.*, 2001, **120**, 30–40.
2 G. Hamscher, S. Sczesny, H. Hoper and H. Nau, *Anal. Chem.*, 2002, **74**, 1509–1518.
3 J. L. Martinez, *Environ. Pollut.*, 2009, **157**, 2893–2902.
4 D. G. J. Larsson, C. de Pedro and N. Paxeus, *J. Hazard. Mater.*, 2007, **148**, 751–755.
5 L. Zhang, J. Tu, L. Lai and C. Hu, *Appl. Catal., B*, 2016, **181**, 561–569.
6 K. Kümmerer, A. Al-Ahmad and V. Mersch-Sundermann, *Chemosphere*, 2000, **40**, 701–710.
7 T. An, H. Yang, G. Li, W. Song, W. J. Cooper and X. Nie, *Appl. Catal., B*, 2010, **94**, 288–294.
8 A. Benito, A. Penadés, J. L. Lliberia and R. Gonzalez-Olmos, *Chemosphere*, 2017, **166**, 230–237.
9 S. W. D. Silva, C. R. Klauck, M. A. Siqueira and A. M. Bernardes, *J. Hazard. Mater.*, 2015, **282**, 241–248.
10 F. C. Moreira, A. R. B. Rui, E. Brillas and V. J. P. Vilar, *Appl. Catal., B*, 2016, **202**, 217–261.
11 S. Giannakis, M. Voumard, D. Grandjean, A. Magnet, L. F. De Alencastro and C. Pulgarin, *Water Res.*, 2016, **2**, 505–515.
12 E. J. Ruiz, C. Arias, E. Brillas, A. Hernandez-Ramirez and J. M. Peralta-Hernandez, *Chemosphere*, 2011, **82**, 495–501.
13 J. Tian, J. Zhao, A. M. Olajuyin, M. M. Sharshar and T. Mu, *Environ. Sci. Pollut. Res.*, 2016, **23**, 1–12.
14 I. Sirés, E. Brillas, M. A. Oturan, M. A. Rodrigo and M. Panizza, *Environ. Sci. Pollut. Res.*, 2014, **21**, 8336–8367.
15 N. Oturan, E. D. van Hullebusch, H. Zhang, L. Mazeas, H. Budzinski, K. Le Menach and M. A. Oturan, *Environ. Sci. Technol.*, 2014, **44**, 2577–2641.
16 F. Sopaj, N. Oturan, J. Pinson, F. Podvorica and M. A. Oturan, *Appl. Catal., B*, 2016, **199**, 331–341.
17 S. Shukla and M. A. Oturan, *Environ. Chem. Lett.*, 2015, **13**, 157–172.
18 E. Brillas, I. Sires and M. A. Oturan, *Chem. Rev.*, 2009, **109**, 6570–6631.
19 Y. Wang, G. Zhao, S. Chai, H. Zhao and Y. Wang, *ACS Appl. Mater. Interfaces*, 2012, **5**, 842–852.
20 S. T. Khankhasaeva, D. V. Dambueva, E. T. Dashinamzhilova, A. Gil, M. A. Vicente and M. N. Timofeeva, *J. Hazard. Mater.*, 2015, **293**, 21–29.
21 T. Liu, K. Wang, S. Song, A. Brouzgou, P. Tsiakaras and Y. Wang, *Electrochim. Acta*, 2016, **194**, 228–238.
22 W. R. P. Barros, J. R. Steter, M. R. V. Lanza and A. C. Tavares, *Appl. Catal., B*, 2015, **180**, 434–441.
23 N. Oturan, J. Wu, H. Zhang, V. K. Sharma and M. A. Oturan, *Appl. Catal., B*, 2013, **140**, 92–97.

24 Y. Wang, Y. Liu, T. Liu, S. Song, X. Gui, H. Liu and P. Tsiakaras, *Appl. Catal., B*, 2014, **156**, 1–7.

25 T. X. H. Le, M. Bechelany, S. Lacour, N. Oturan, M. A. Oturan and M. Cretin, *Carbon*, 2015, **94**, 1003–1011.

26 W. H. Wang, X. D. Wang, W. H. Wang and X. D. Wang, *Electrochim. Acta*, 2007, **52**, 6755–6762.

27 S. Ding, F. Liu, X. Shi and H. He, *Appl. Catal., B*, 2016, **180**, 766–774.

28 Q. Wang, Y. Li, B. Liu, Q. Dong, G. Xu, L. Zhang and J. Zhang, *J. Mater. Chem. A*, 2015, **3**, 139–147.

29 M. Jing, X. Zhang, X. Fan, L. Zhao, J. Liu and C. Yan, *Electrochim. Acta*, 2016, **215**, 57–65.

30 J. Tian, J. Zhao, A. M. Olajuyin, M. M. Sharshar, T. Mu, M. Yang and J. Xing, *Environ. Sci. Pollut. Res.*, 2016, **23**, 15471–15482.

31 K. V. Plakas, S. D. Sklari, D. A. Yiankakis, G. T. Sideropoulos, V. T. Zaspalis and A. J. Karabelas, *Water Res.*, 2016, **91**, 183–194.

32 M. Sun, X. R. Ru and L. F. Zhai, *Appl. Catal., B*, 2015, **165**, 103–110.

33 H. Zhou, Y. Shen, J. Xi, X. Qiu and L. Chen, *ACS Appl. Mater. Interfaces*, 2016, **8**, 15369–15378.

34 C. Pham-Huu, R. Vieira, B. Louis, A. Carvalho, J. Amadou, T. Dintzer and M. J. Ledoux, *J. Catal.*, 2006, **240**, 194–202.

35 A. L. Chen, Y. Zhou, N. Ta, Y. Li and W. J. Shen, *Catal. Sci. Technol.*, 2015, **5**, 4184–4192.

36 Y. Li, Y. N. Li, B. R. Xie, J. J. Han, S. H. Zhan and Y. Tian, *Environ. Sci.: Nano*, 2017, **4**, 425–436.

37 L. Wang, H. Liu, Y. Liu, Y. Chen and S. Yang, *J. Rare Earths*, 2013, **31**, 559–564.

38 L. Yue, W. Li, F. Sun, L. Zhao and L. Xing, *Carbon*, 2010, **48**, 3079–3090.

39 L. Tu, S. C. Chang and J. F. Peng, *Thin Solid Films*, 2010, **518**, 5488–5493.

40 Y. W. Zhang, R. Si, C. S. Liao and C. H. Yan, *J. Phys. Chem. B*, 2003, **107**, 10159–10167.

41 L. Qi, Q. Yu, Y. Dai, C. J. Tang, L. J. Liu, H. L. Zhang, F. Gao, L. Dong and Y. Chen, *Appl. Catal., B*, 2012, **119**, 308–320.

42 P. V. R. Rao, V. P. Kumar, G. S. Rao and K. V. R. Chary, *Catal. Sci. Technol.*, 2012, **2**, 1665–1673.

43 S. Mahammadunnisa, P. M. K. Reddy, N. Lingaiah and C. Subrahmanyam, *Catal. Sci. Technol.*, 2012, **3**, 730–736.

44 M. M. Antunes, S. Lima, P. Neves, A. L. Magalhães, E. Fazio, F. Neri, M. T. Pereira, A. F. Silva, C. M. Silva, S. M. Rocha, M. Pillinger, A. Urakawa and A. A. Valente, *Appl. Catal., B*, 2016, **182**, 485–503.

45 G. Zhou, H. Lan, T. Gao and H. Xie, *Chem. Eng. J.*, 2014, **246**, 53–63.

46 D. Srinivas, C. V. V. Satyanarayana, H. S. Potdar and P. Ratnasamy, *Appl. Catal., A*, 2003, **246**, 323–334.

47 F. Sopaj, N. Oturan, J. Pinson, F. Podvorica and M. A. Oturan, *Appl. Catal., B*, 2016, **199**, 331–341.

48 D. M. de Araujo, C. Saez, C. A. Martinez-Huitle, P. Canizares and M. A. Rodrigo, *Appl. Catal., B*, 2015, **166**, 454–459.

49 Y. M. Liu, S. Chen, X. Quan, H. T. Yu, H. M. Zhao and Y. B. Zhang, *Environ. Sci. Technol.*, 2015, **49**, 13528–13533.

50 E. Brillas, I. Sirés and M. A. Oturan, *Chem. Rev.*, 2009, **109**, 6570–6631.

51 A. Özcan, Y. Sahin, A. S. Koparal and M. A. Oturan, *J. Electroanal. Chem.*, 2008, **616**, 71–78.

52 S. Ammar, M. A. Oturan, L. Labiadh, A. Guersalli, R. Abdelhedi, N. Oturan and E. Brillas, *Water Res.*, 2015, **74**, 77–87.

53 A. Khataee, A. Khataee, M. Fathinia, B. Vahid and W. J. Sang, *J. Ind. Eng. Chem.*, 2013, **19**, 1890–1894.

54 N. Barhoumi, L. Labiadh, M. A. Oturan, N. Oturan, A. Gadri, S. Ammar and E. Brillas, *Chemosphere*, 2015, **141**, 250–257.

55 W. R. P. Barros, J. R. Steter, M. R. V. Lanza and A. C. Tavares, *Appl. Catal., B*, 2016, **180**, 434–441.

56 V. S. Antonin, M. C. Santos, S. Garcia-Segura and E. Brillas, *Water Res.*, 2015, **83**, 31–41.

57 J. S. Ye, J. Liu, H. S. Ou and L. L. Wang, *Chemosphere*, 2016, **165**, 311–319.

58 J. Zbiljić, O. Vajdle, V. Guzsvány, J. Molnar, J. Agbaba, B. Dalmacija and K. Kalcher, *J. Hazard. Mater.*, 2014, **283**, 292–301.

59 N. W. Beyene, P. Kotzian, K. Schachl, H. Alemu, E. Turkusic, A. Chopra, H. Moderegger, I. Svancara, K. Vytras and K. Kalcher, *Talanta*, 2004, **64**, 1151–1159.

60 K. Schachl, H. Alemu, K. Kalcher, J. Jezkova, I. Svancara and K. Vytras, *Analyst*, 1997, **122**, 985–989.